American Journal of Water Resources, 2026, Vol. 14, No. 3, 83-96
Available online at http://pubs.sciepub.com/ajwr/14/3/4
Published by Science and Education Publishing
DOI:10.12691/ajwr-14-3-4

Hydrogeochemical Assessment of Groundwater and Surface Water under Environmental Pressures: Case Study of the Mô Basin, Togo

Kossi TCHAPO[1,2,*], Kossitse Venyo AKPATAKU[1,2], Lallébila TAMPO[1,2], Agbessi Koffi SODOMON[1], Bouwèdéou ALIDOU[1], Moudassirou SEDOU[1], Seyf-Laye ALFA-SIKA MANDE[1,2]

[1]Laboratory of Organic Chemistry and Environmental Sciences, Department of Chemistry, University of Kara, P.O. Box: 404, Kara, Togo
[2]Laboratory of Applied Hydrology and Environment, Department of Chemistry, University of Lomé, P.O. Box: 1515, Lomé, Togo
*Corresponding author: tchapok1988@gmail.com

Received October 10, 2026; Revised November 12, 2026; Accepted November 20, 2026

Abstract This study presents the first comprehensive hydrochemical characterization of water resources in the Mô Basin (central-western Togo) to identify the factors controlling water chemistry, assess water quality for drinking and irrigation, and identify areas most vulnerable to anthropogenic impacts. We collected 150 water samples (132 groundwater samples from 44 boreholes and 18 surface water samples from 6 monitoring stations) across three hydrological periods (low-flow, high-flow, and transition). Physicochemical parameters and major ions were analyzed in accordance with AFNOR standard methods. The dataset was interpreted using descriptive statistics, multivariate statistical analyses, hydrochemical diagrams, and irrigation water quality indices. Groundwater exhibits significantly higher mineralization than surface water, with a mean electrical conductivity of 456.73 ± 227.35 µS/cm compared with 110.20 ± 114.38 µS/cm, reflecting longer water–rock interaction within the aquifer. Water chemistry is dominated by the Ca-Mg-HCO_3 hydrochemical facies, which is characteristic of crystalline bedrock aquifers. Approximately 70% of the groundwater samples are classified as hard to very hard; however, the concentrations of all analyzed parameters remain within the World Health Organization (WHO) guidelines. Nitrate concentrations range from 0 to 14.70 mg/L in groundwater and up to 16.55 mg/L in surface water, while phosphate concentrations range from 0.01 to 2.00 mg/L, although localized enrichments occur in areas of intensive agricultural activity and high population density. Multivariate statistical analyses indicate that water chemistry is primarily controlled by silicate weathering and water-rock interactions, whereas anthropogenic inputs exert only a localized secondary influence on selected chemical parameters. Groundwater generally complies with WHO drinking water guidelines for all parameters investigated, whereas surface water frequently exceeds the recommended turbidity limits. Irrigation water quality indices indicate that most samples fall within classes suitable for agricultural use, with a low risk of soil salinization and sodification.

Keywords: *Hydrogeochemical assessment, groundwater, surface water, environmental pressures*

Cite This Article: Kossi TCHAPO, Kossitse Venyo AKPATAKU, Lallébila TAMPO, Agbessi Koffi SODOMON, Bouwèdéou ALIDOU, Moudassirou SEDOU, and Seyf-Laye ALFA-SIKA MANDE, "Hydrogeochemical Assessment of Groundwater and Surface Water under Environmental Pressures: Case Study of the Mô Basin, Togo." *American Journal of Water Resources*, vol. 14, no. 3 (2026): 83-96. doi: 10.12691/ajwr-14-3-4.

1. Introduction

The availability of high-quality water resources is one of the major challenges to sustainable development, particularly in developing countries, where rapid population growth, urban expansion, agricultural intensification, and the impacts of climate change are placing increasing pressure on water resources [1,2]. Groundwater and surface water are the primary sources of water supply for domestic, agricultural, and industrial purposes [3,4]. However, their quality is continuously influenced by natural processes, including the weathering of geological formations, water-rock interactions, and climatic variability, as well as by anthropogenic pressures such as intensive agriculture, domestic wastewater discharges, and inadequate sanitation infrastructure [5,6,7,8].

In West Africa, sustainable water resource management remains a major challenge in a context characterized by high climatic variability and increasing human pressure. Numerous hydrochemical studies conducted across the subregion have shown that water chemistry results from complex interactions among geological settings, geochemical processes, and anthropogenic activities [8,9,10,11,12]. These studies have consistently

demonstrated that rock weathering is the dominant process controlling water mineralization while also highlighting the localized effects of agricultural practices and domestic wastewater discharges on water quality degradation[13].

In Togo, water resources play a crucial role in socioeconomic development, food security, and living conditions. Although several studies have investigated water quality in selected watersheds and aquifers across the country, significant knowledge gaps remain, particularly in the Mô Basin [11,12]. Located in central-western Togo, this basin isimportant because it supports rural water supply, agro-pastoral activities, and ecosystem conservation within the Fazao-Malfakassa Wildlife Reserve. Local communities depend largely on groundwater and surface water to meet domestic needs, irrigate crops, water livestock, and sustain various economic activities [14,15].

Despite the strategic importance of the Mô Basin, scientific knowledge of its water quality, hydrochemical characteristics, and the processes governing water chemistry remains limited [16,17]. In particular, few studies have jointly investigated groundwater and surface water, integrating hydrochemical facies identification, geochemical process characterization, and water quality assessmentagainst international drinking water and irrigation standards [18,19]. This lack of comprehensive information limits our understanding of the basin's hydrochemical functioning and constrains the development of effective strategies for the sustainable management and protection of its water resources [20,21].

To address these knowledge gaps, this study aims to characterize the hydrochemical properties of groundwater and surface water in the Mô Basin. Specifically, the objectives are to determine the physicochemical characteristics of the water resources;identify the major hydrochemical facies and the natural and anthropogenic processes controlling their evolution; assess water quality against international guidelines for drinking and irrigation purposes; and identify areas potentially vulnerable to water quality degradation [22]. The findings of this study provide new insights into the hydrochemical functioning of one of the least-studiedwatersheds in Togo and provide a scientific basis for sustainable water resource management, the implementation of appropriate protection measures, and informed decision-making by water resource managers and policymakers.

2. Materials and Methods

2.1. Description of the Study Area

The Mô watershed lies in west- central Togo, about 380 km north of Lomé. As a major sub-basin of the Volta River system, it spans latitudes 8°38′-9°30′N and longitudes0°21′-1°18′E, covering 5618 km^2, roughly 9.9% of the national territory (Figure 1). Administratively, the catchment includes the prefectures ofMô-Plaine, Bassar, Tchaoudjo and part of Sotouboua. The hydrographic network is dominated by the Mô River, which originates in the Alédjo- Kadara mountains and drains into the Volta Basin. Its mean annual discharge is about 20 m^3/s, with seasonal peaks up to 80 m^3/s [23]. Over nearly 37 km, the river forms the natural western boundary between Togo and Ghana. The regional topography, developed over a Precambrian crystalline basement, is rugged, with elevations ranging from 224 to 722 m above sea level. Prominent orographic features include the Alédjo-Kadara, Fazao-Malfakassa, and Tchaoudjo massifs. Geologically, the basin belongs to the Pan- African Dahomeyides orogenic belt and is dominated by the Atacorean and Buem structural units. These formations primarily consist of quartzites, schists, quartzitic sandstones, and arkoses, interlayered with sedimentary and metamorphic rock assemblages that reflect a complex tectonic evolution [23,24,25]. From a hydrogeological perspective, the catchment features a dual aquifer system: an upper, shallow, unconfined aquifer developed within the weathered granito-gneissic saprolite layer, and a deeper, underlying semi-confined to confined aquifer hosted within the fractured crystalline basement rocks [26,27,28]. The basin experiences a Sudanian-Guinean tropical climate, with a distinct rainy season from May to October and a dry season from November to March. The annual rainfall is about 1,200 mm, and the mean annualtemperature is around 28°C [27]. These hydroclimatic boundary conditions fundamentally govern local hydrological processes, soil erosion rates, and groundwater recharge dynamics. In recent decades, this hydrogeological system has faced escalating anthropogenic environmental pressures [28]. Rapid population growth, transhumant livestock farming, and agricultural intensification (notably cash crop cultivation) induce significant diffuse and point-source pollution hazards [27,28,29,30]. Consequently, the interplay among climate, steep topography, complex lithology, and human activities makes the Mô watershed a compelling natural laboratory for investigating hydrogeochemical processes under shifting environmental conditions.

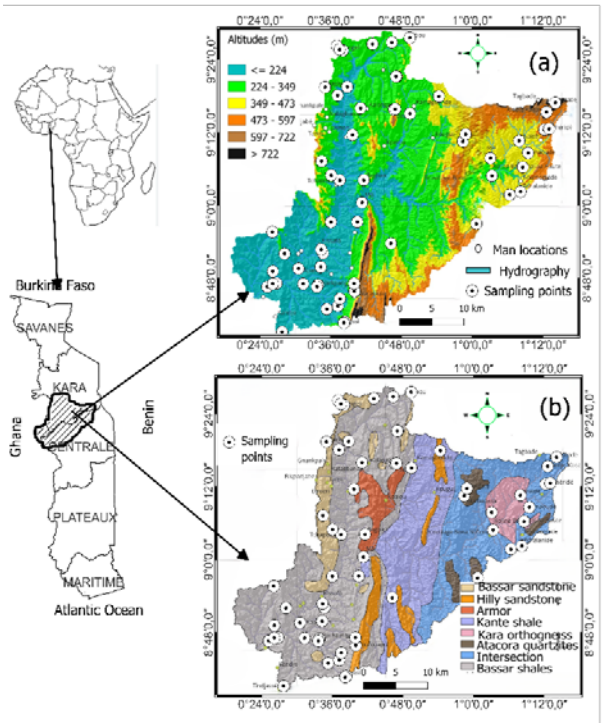


Figure 1. Location, hypsometric (a) and geological (b) maps of the Mô Basin showing the sampling sites

2.2. Sampling Strategy and Data Collection

Sampling points were selected based on a comprehensive well inventory provided by the Regional Directorate of Water Resources, which was subsequently updated and validated through an extensive field survey to verify the operational status of each installation [31]. Sampling was conducted across50 monitoring sites-comprising 44 representative boreholes (with screen depths ranging from 6 to 50 m) and 6 surface water stations-over three distinct seasonal campaigns. This sampling design yielded a total of 150 water samples, consisting of 132 groundwater samples (44 boreholes× campaigns) and 18 surfacewater samples (6 stations × campaigns), effectively covering the basin's primary geological units and hydrogeological settings.

To evaluate the seasonal variability of water quality under changing environmental pressures, the three monitoring campaigns were conducted during critical phases of the local hydrological cycle: the low-flow period (dry season), the high-flow period (rainy season), and the hydrological transition period [32].

To ensure compliance with international quality standards, all sampling, preservation, and handling procedures strictly followed the NF EN ISO 5667-1, 5667-3, and 5667-6 guidelines [21,33]. Before groundwater collection, boreholes were purged for approximately 15 to 20 minutes to eliminate stagnant casing water, and sampling was conducted only after the stabilization of physical indicator parameters.

In situ parameters, including water temperature (T °C), pH, electrical conductivity (EC, µS/cm), and dissolved oxygen (DO,mg/L), were measured immediately on-site.These measurements were performed using a calibrated Hanna Instruments HI98129 Combo multi-parameter portable probe, which was systematically calibrated at the beginning of each sampling day with certified buffer solutions. TheWater samples were collected in 1-liter high-density polyethylene bottles. In accordance with preservation protocols, these bottles were washed in the laboratory with 10% nitric acid, rinsed with deionized water, and then conditioned on-site by rinsing them three times with the water to be sampled. The bottles intended for the analysis of major cations (Ca^{2+}, Mg^{2+}, Na^{+}, and K^{+}) were filtered through 0.45 µm cellulose acetate membranes and immediately acidified to pH < 2 with ultrapure nitric acid (HNO_3) to prevent precipitation and metal adsorption. Bottles dedicated to the analysis of major anions (HCO_3^-, Cl^-, and SO_4^{2-}) were filtered but not acidified. All samples were stored and transported to the laboratory in accordance with AFNOR protocols [33].

2.3. Analytical Techniques and Quality Assurance

Laboratory analyses were performed using standardized analytical methods, in accordance with the protocols of the French Standardization Association. Dissolved concentrations of calcium, magnesium, bicarbonates, Chlorides, sulfates, orthophosphates, nitrates, and siliconwere determined using a METASH 5200 computerized molecular absorption spectrophotometer. Sodium and potassium concentrations were analyzed using a Jenway flame atomic absorption spectrophotometer. Total alkalinity and bicarbonate concentrations were determined upon receipt of the samples by standard acid-base volumetric titration with hydrochloric acid.

The internal consistency of each hydrochemical analysis was confirmed by calculating the ion balance error (IBE), expressed as a percentage, where all major cation and anion concentrations were converted to milliequivalents per liter (meq/L):

$$\mathrm{IBE}(\%) = \left(\frac{\sum \mathrm{Cations} - \sum \mathrm{Anions}}{\sum \mathrm{Cation} + \sum \mathrm{Anions}} \right) \times 100 \qquad (1)$$

Only hydrochemical analyses with a strict ion balance errorwithin ±5% were included in the geochemical interpretation.

2.4. Hydrogeochemical Modeling and Statisticaldata Processing

The data were analyzed using descriptive statistics and multivariate methods, including principal component analysis (PCA) and ascending hierarchical clustering (AHC) [34,35]. Hydrochemical facies were determined using Piper and Durov diagrams. Gibbs diagrams were used to distinguish rock weathering, evaporation, and atmospheric precipitation. Binary diagrams: $Ca^{2+} + Mg^{2+} = f\left(HCO_3^-\right)$; $(Ca^{2+} + Mg^{2+}) = f\left(HCO_3^- + SO_4^{2-}\right)$ and Gaillardet diagrams; $NO_3^- / Cl^- = f\left(Cl^-\right)$; $(Ca^{2+} + Mg^{2+}) - \left(HCO_3^- + SO_4^{2-}\right) = f\left(Na^+ - Cl^-\right)$ were used to identify carbonate dissolution or silicate weathering specific to the bedrock. Principal Component Analysis (PCA) coupled with Ascending Hierarchical Classification (AHC) was applied to distinguish natural hydrogeochemical signatures (geogenic origin) from chemical anomalies induced by anthropogenic pressures (pesticides, nitrogen fertilizers, domestic wastewater)

2.5. Water Quality Assessment for Drinking and Irrigation Purposes

The suitability of both surface and groundwater for human consumption was assessed by direct comparison with the World Health Organizationguideline values [36]. For agricultural suitability, specific sodicity and salinity hazards were evaluated using standard irrigation indices calculated from concentration values in meq/L.

Sodium Adsorption Ratio (SAR):

$$\mathrm{SAR} = \left(\frac{Na^+}{\sqrt{\frac{Ca^{2+} + Mg^{2+}}{2}}} \right) \qquad (2)$$

Sodium Percentage (%Na):

$$\%Na = \left(\frac{Na^+ + K^+}{Ca^{2+} + Mg^{2+} + Na^+ + K^+} \right) \quad (3)$$

Residual Sodium Carbonate (RSC):

$$RSC = HCO_3^- - \left(Ca^{2+} + Mg^{2+} \right) \quad (4)$$

3. Results and Discussion

3.1. Physicochemical Parameters Measured In Situ

3.1.1. Temperature and Dissolved Oxygen

The average groundwater temperatures were 29.29°C, 28.33°C, and 29.96°C during the three sampling campaigns (Tables 1-3). Surface water temperatures were slightly higher, with mean values of 30.10°C, 29.30°C, and 30.75°C, respectively. This difference is attributed to the direct exposure of surface waters to solar radiation, whereas groundwater temperatures are buffered by the surrounding aquifer materials, which limit thermal fluctuations. Most borehole temperatures ranged between 27 and 29°C, values close to the mean air temperature recorded during the sampling campaigns (≈ 28°C). This narrow temperature range indicates relatively stable thermal conditions within the aquifers, while the higher surface water temperatures reflect greater sensitivity to seasonal climatic variations.

Dissolved oxygen (DO) concentrations differ markedly between groundwater and surface water. Surface waters exhibit higher average DO concentrations of 6.09 mg/L during the high-flow period and 7.11 mg/L during the transition period, reflecting continuous atmospheric exchange as well as the effects of water turbulence and photosynthetic activity. In contrast, groundwater shows lower DO concentrations, averaging 3.17 mg/L during the low-flow period and 2.73 mg/L during the high-flow period. These low values are consistent with the confined nature of the aquifers, longer residence times, and oxygen consumption through biological and geochemical processes [37].

Approximately 83% of surface water samples exhibit DO concentrations above 4 mg/L, indicating generally well-oxygenated conditions. In contrast, only 37% of groundwater samples exceed this threshold. At the same time, a significant proportion shows concentrations below 2 mg/L, which is characteristic of low-oxygen environments where reducing conditions and redox-sensitive processes may become dominant.

3.1.2. Turbidity and Hydrogen Potential (pH).

Turbidity values measured in most groundwater samples during the three sampling campaigns remained below the World Health Organization (WHO) guideline value for drinking water (5 NTU). In contrast, surface water exhibited considerably higher turbidity, with mean values ranging from 27.67 to 97.78 NTU. This marked difference reflects surface water's direct exposure to runoff and soil erosion, processes intensified by agricultural activities, deforestation, and urbanization.

Groundwater pH values ranged from 5.0 to 8.0, whereas surface water pH ranged from 6.0 to 8.5. Most samples fell within the WHO-recommended pH range for drinking water (6.5-8.5). However, pH values below 6.5 were observed mainly in aquifers developed within quartzites, sandstones, and orthogneissesand were generally associated with low electrical conductivity values (Figure 2a and 2b). This relationship suggests low water mineralization resulting from the limited weathering potential of these silicate-rich lithologies and reduced water-rock interactions. In addition, the dissolution of soil-derived CO_2 and the infiltration of weakly mineralized meteoric water may also contribute to the observed acidity [38,39]. These findings are consistent with those reported by others who documented the predominance of acidic groundwater in central Togo.

Figure 2a and Figure 2b show that the lowest pH values are concentrated mainly in the eastern part of the basin, corresponding to the Atakora structural unit, whereas pH values between 6.5 and 8.0 predominate within the Buem geological series. This spatial pattern highlights the influence of lithology on the water's hydrochemical characteristics. In addition, several agricultural and urbanized areas are located within zones where the pH is below 7.0. Although this spatial association does not demonstrate a causal relationship, it may indicate a localized influence of anthropogenic activities on groundwater acidity, which warrants further investigation

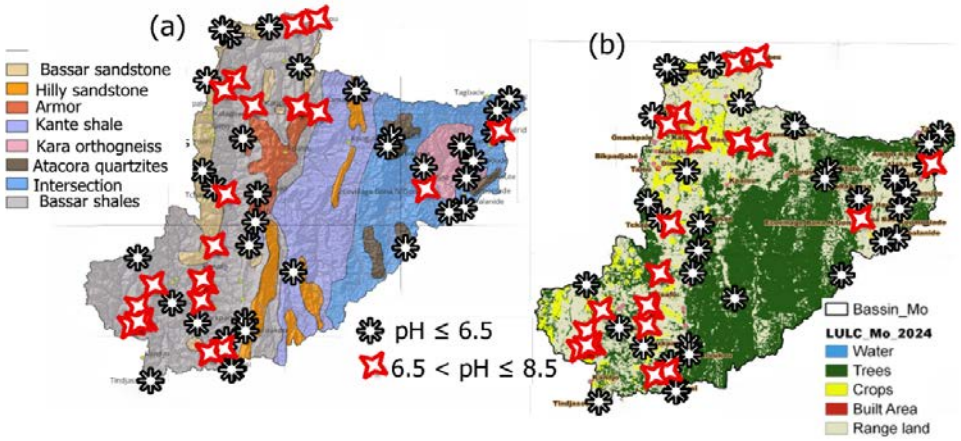


Figure 2. Spatial distribution of pH: (a) overlaid on the geological map; (b) overlaid on the land-use map

Table 1. Descriptive statistics for the variables measured in groundwater and surface water during low-flow periods

Vars	Groundwater				Surface water			
	Min	Max	Average	St.Dev	Min	Max	Average	St.Dev
TDS(mg/L)	12	550	228.79	143.34	50.00	277	210	74.36
Temperature (°C)	27	32	29.29	1.08	28.30	32	30.10	1.85
pH	5	8	6.96	0.65	5.76	7.76	7.04	1.11
EC (µS/cm)	20	1080	434.15	245.99	71	331	120	190.53
DO (mg/L)	2	6	3.17	2.81	3.88	10.50	6.96	2.85
Turb (NTU)	0.10	66	6.18	14.63	3.81	97.51	58.86	0.92
Ca^{2+}(mg/L)	2	90	34.38	18.79	6.40	12.00	9.20	4.80
Mg^{2+}(mg/L)	1	65	17.56	13.37	4.86	9.23	7.45	2.30
Na^{+}(mg/L)	1	67	21.59	15.36	1.20	3.20	1.97	1.08
K^{+}(mg/L)	0.20	14	4.95	3.17	4.10	11.50	6.63	4.22
HCO_3^-(mg/L)	8	390	160.69	105.05	17.08	48.19	27.45	17.96
Cl^-(mg/L)	1	71	11.00	9.93	7.09	11.34	9.22	3.00
SO_4^{2-}(mg/L)	<LD	18	1.81	3.74	<LD	0.74	0.25	0.42
NO_3^-(mg/L)	<LD	14.70	7.43	3.91	0.57	16.55	8.52	9.56
PO_4^{3-}(mg/L)	0.10	1	0.17	0.16	0.08	0.28	0.15	0.11

Table 2. Descriptive statistics for the variables measured in groundwater and surface water during flood events

Vars	Groundwater				Surface water			
	Min	Max	Average	St.Dev	Min	Max	Average	St.Dev
TDS(mg/L)	13	581	228.12	135.38	32	42	35	11.27
Temperature (°C)	26	31	28.33	1.01	26	31.40	29.30	2.89
pH	5	8	6.80	0.71	7.40	7.90	7.62	0.25
EC (µS/cm)	10	990	446.88	268.07	40	80	67.27	23.09
DO (mg/L)	0.1	5	2.73	0.75	3.45	9.20	6.29	0.97
Turb NTU	0.13	34	4.13	6.76	11.60	27.67	17.03	5.55
Ca^{2+}(mg/L)	5	74	38.20	17.60	4.00	19.20	9.867	8.17
Mg^{2+}(mg/L)	1.45	47	19.19	11.78	2.43	6.80	4.21	2.30
Na^{+}(mg/L)	1	38	18.04	9.49	4.10	4.50	4.27	0.21
K^{+}(mg/L)	0.2	11	4.08	2.18	1.10	1.20	1.13	0.06
HCO_3^-(mg/L)	23	490	233.19	119.84	34.16	56.12	47.58	11.77
Cl^-(mg/L)	3	125	22.65	7.05	7.10	17.75	10.65	6.15
SO_4^{2-}(mg/L)	<LD	19	1.65	4.09	0.00	0.00	0.00	0.00
NO_3^-(mg/L)	<LD	9	1.50	2.41	1	5.12	2.05	1.06
PO_4^{3-}(mg/L)	<LD	2	0.06	0.11	<LD	<LD	<LD	0.00
F^-(mg/L)	<LD	1.5	0.23	0.11	0.09	0.14	0.11	0.02

Table 3. Descriptive statistics for the variables measured in groundwater and surface water during the transition period

Vars	Groundwater				Surface water			
	Min	Max	Average	St.Dev	Min	Max	Average	St.Dev
TDS(mg/L)	13	848	285.75	179.62	32	150	84.33	40.67
Temperature (°C)	27	34	29.96	1.45	28	36	30.75	2.71
pH	5	8	6.65	0.68	6.70	8.30	7.49	0.93
EC (µS/cm)	40	1090	489.18	168	60	329	143.33	129.52
DO (mg/L)	2	6	2.92	1.25	4.23	11.21	7.11	2.37
Turb (NTU)	0	19	2.37	3.35	8	630	97.78	200.84
Ca^{2+}(mg/L)	3	64	33.08	14.85	6	14	10.17	8.87
Mg^{2+}(mg/L)	6	52	23.86	12.21	2	13	8.22	3.35
Na^{+}(mg/L)	2	159	36.22	32.82	5	13	4.75	2.96
K^{+}(mg/L)	0	21	3.38	2.86	2	46	11.56	13.13
HCO_3^-(mg/L)	77	369	153.83	50.89	82	149	113.11	22.60
Cl^-(mg/L)	3	145	17.31	9.82	9	46	21.56	10.62
SO_4^{2-}(mg/L)	<LD	143	10.59	19.85	0.42	14	2.22	2.30
NO_3^-(mg/L)	<LD	11	1.91	2.03	1	9	4.22	2.59
Fe	<LD	1	0.01	0.02	<LD	<LD	<LD	0.00
SiO_2(mg/L)	1	56	26.76	13.24	<LD	12	5.25	4.92

Var = variables ; Min = minimum; Max = maximum ; Avg = average ;St. Dev = standard deviation ; LD = limit of detection ; pH= hydrogen potential (unitless).

3.1.3. Electrical Conductivity and Total Dissolved Solids

Theaverage electrical conductivities of groundwater range from 434.15 to 489.18 µS/cm, while those of surface water range from 67.27 to 143.33 µS/cm. These results reflect significantly higher groundwater mineralization and prolonged interactions between water and geological formations. The spatial distribution of conductivity reveals variability within a single geological unit (Figure 3a), indicating that water mineralization depends not only on the nature of the rocks through which the water flows, but also on local water flow conditions and weathering processes. The highest conductivity values are mainly observed in areas dominated by sandstone and quartzite, where longer residence time could promote mineral dissolution. Overlaying the conductivity data on land use (Figure 3b) shows that the highest values are also concentrated in heavily cultivated and densely populated areas. This distribution suggests that agricultural activities, particularly the use of mineral fertilizers and domestic wastewater discharges, may contribute to the enrichment

of water with ions, in addition to natural rock weathering processes [40,41].

These values confirm the diversity of mineralization levels observed in the basin. The highest concentrations are likely associated with increased water-rock interactions, evaporation-induced concentration during dry periods, and, locally, human activities.

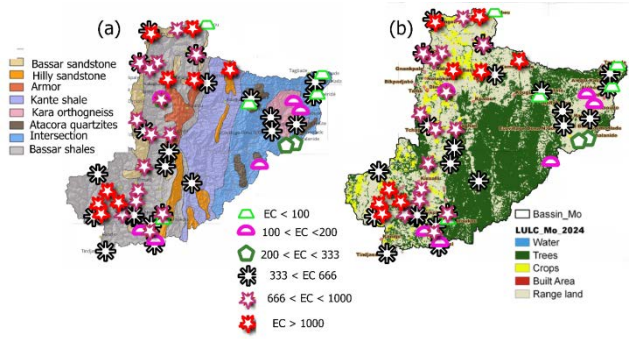


Figure 3. Spatial distribution of electrical conductivity: (a) overlaid on the geological map; (b) overlaid on the land-use map

3.2. Ionic Composition and Hydrochemical Facies

3.2.1. Major Cations

During the three sampling campaigns, the average concentrations of Ca^{2+} in the groundwater ranged from 33.08 to 38.20 mg/L, Mg^{2+} from 17.56 to 23.86 mg/L, Na^{+} from 18.04 to 36.22 mg/L, and K^{+} from 3.38 to 4.95mg/L. In surface water, the average concentrations ranged from 9.20 to 10.17 mg/L for Ca^{2+}, from 4.21 to 8.22 mg/L for Mg^{2+}, from 1.97 to 4.75 mg/L for Na^{+}, and from 1.13 to 11.56 mg/L for K^{+}. Calcium and magnesium concentrations are consistently higher in groundwater than in surface water, reflecting greater mineral dissolution during subsurface flow, which is consistent with typical bedrock aquifer processes.

Total hardness, calculated from calcium and magnesium concentrations and expressed in mg $CaCO_3$/L, shows that 49% of wells produce hard water and 21% produce very hard water, meaning that approximately 70% of the groundwater samples fall into the hard to very hard categories (> 150 mg/L; Table 4). This pattern is driven by high spatial variability and a wide standard deviation in individual ionic levels across sampling points. This high hardness is consistent with a significant contribution of alkaline earth metal ions to the chemical composition of groundwater. While hard water generally does not pose a health risk, it can promote scale formation in distribution systems and household appliances.

Sodium and potassium concentrations remain relatively low compared to calcium and magnesium. However, a few elevated values observed locally-particularly for potassium in certain surface waters-indicate spatial variability that may reflect the combined influence of local geological characteristics and human activities.

Table 4. Classification of waters based on their hardness

Water hardness in mg $CaCO_3$/L	Water quality	Percentage (%) of wells
[0 - 75[	Very soft water	7 %
[75 - 150[	Moderately soft water	24 %
[150 - 300[	Hard water	49 %
[300 and above [	Very hard water	21 %

3.2.2. Major Anions

Bicarbonates (HCO_3^-) are the predominant anion in both groundwater and surface water. The average concentrations of HCO_3^-, Cl^-, SO_4^{2-} and NO_3^- are 160.69-233.19 mg/L, 11.00-22.65 mg/L, 1.65-10.59 mg/L, and 1.50-7.43 mg/L in groundwater, compared to 27.45-113.11 mg/L, 9.22-21.56 mg/L, 0-2.22 mg/L, and 2.05-8.52 mg/L in surface water. Thepredominance of bicarbonates indicates the role of silicate mineral dissolution reactions and chemical weathering processes in water mineralization, as is commonly observed in aquifers developed within the crystalline basement. Chloride and sulfate concentrations remain low in most samples and are well below WHO guidelines for water intended for human consumption [42]. Nitrate concentrations remain generally low across the basin, ranging overall from 0 to 14.70 mg/L in groundwater and up to 16.55 mg/L in surface water (Table 1- Table 3), with localized peak values observed during the low-flow period in agricultural sectors and densely populated areas. Although all measured concentrations remain below the WHO-recommended guideline value of 50 mg/L, this spatial variability suggests a local influence of human activities on water quality.

The average order of abundance of ions is $Ca^{2+} > Mg^{2+} \approx Na^{+} > K^{+}$ for cations and $HCO_3^- > Cl^- > SO_4^{2-} > NO_3^-$ for anions in groundwater; surface waters generally exhibit the sequence $Ca^{2+} > Mg^{2+} > K^{+} > Na^{+}$ for cations and $HCO_3^- > Cl^- > NO_3^- > SO_4^{2-}$ for anions. These sequences demonstrate the significant contribution of alkaline earth metals and bicarbonates to the chemical composition of the waters in the studied basin.

Orthophosphate (PO_4^{3-}) concentrations were generally below the limit of detection (<LD) or very low (< 0.2 mg/L) in most samples.However, a few higher values were observed sporadically. The low concentrations observed are consistent with the low mobility of phosphates in soils, due to their adsorption onto iron and aluminum oxides and clay minerals. The few instances of elevated concentrations observed could be associated with local inputs from agricultural sources or domestic discharges.

3.3. Multivariate Statistical Analyses

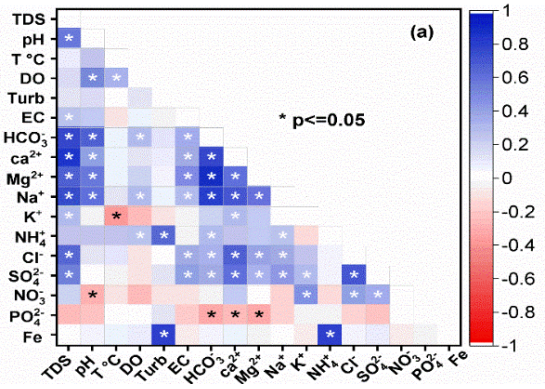
3.3.1. Relationships Between Variables

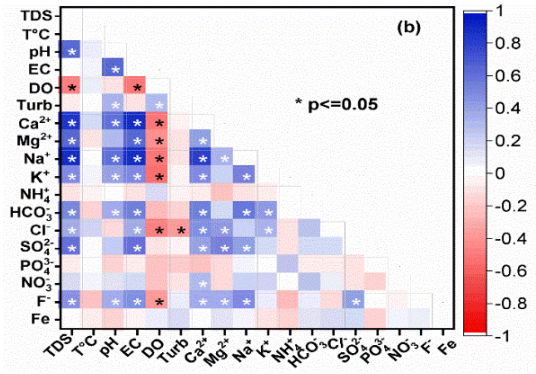
Pearson's correlation analysis was used to examine

relationships between physicochemical parameters and major ions,and to identify processes that may influence the chemical composition of the water [43]. The correlation coefficients are presented in Figure 4; only significant correlations ($p < 0.05$) were included in the interpretation.

Across the three monitoring campaigns, electrical conductivity (EC) and total dissolved solids (TDS) exhibited strong positive correlations with the major dissolved ions, including Ca^{2+}, Mg^{2+}, Na^{+}, and HCO_3^-, indicating that these species are the principal contributors to groundwater mineralization. The strong association between EC, bicarbonate, and alkaline earth cations suggests that groundwater chemistry is primarily controlled by mineral dissolution and water-rock interactions characteristic of crystalline bedrock aquifers. Positive correlations between EC and Cl^-, SO_4^{2-}, Na^+, and K^+ were also observed during some monitoring campaigns, reflecting the contribution of these ions to the overall dissolved ionic load. However, correlation analysis alone is insufficient to distinguish between geogenic and anthropogenic sources of these constituents, highlighting the need for complementary hydrochemical indicators and geochemical interpretation [44]. Negative correlations between dissolved oxygen and selected parameters, particularly turbidity and, where available, total iron, suggest that redox conditions exert a significant control on iron mobility within the aquifer. This pattern is consistent with the oxidation of dissolved ferrous iron and the subsequent precipitation of iron oxyhydroxides under more oxidizing conditions.

The positive correlation between dissolved silica (SiO_2) and alkali metals (Na^+ and K^+) is consistent with the weathering of silicate minerals, which constitutes the principal natural source of dissolved silica in groundwater. Correlations involving nutrients (NO_3^-, PO_4^{3-}, and NH_4^+) exhibited marked seasonal variability, suggesting episodic inputs from surface processes, including runoff and anthropogenic activities. Although these inputs may locally influence groundwater chemistry, they do not appear to be the dominant controls on groundwater mineralization. Overall, the observed correlation patterns indicate that groundwater chemistry is primarily governed by water-rock interactions, while anthropogenic inputs exert a secondary, localized influence.





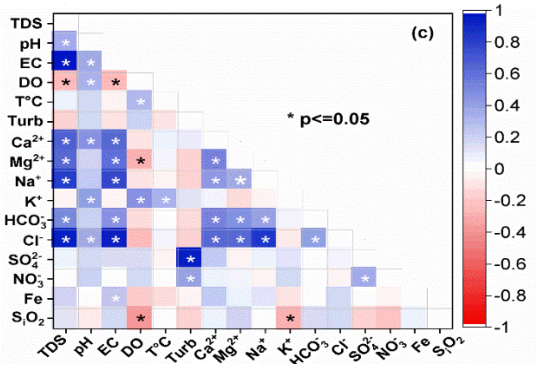


Figure 4. Pearson's correlations between the variables

3.3.2. Principal Component Analysis (PCA)

Principal component analysis (PCA) was performed on the data from the three sampling campaigns after verifying their suitability (KMO: 0.71- 0.76; Bartlett's test, $p < 0.001$). Based on the Kaiser criterion (eigenvalue > 1), two components were selected for the C-I campaign and three for the C-II and C-III campaigns. The extracted factors explain 70.84%, 75.12%, and 71.06% of the total variance, respectively (Table 5).

Across all three sampling campaigns, the first principal component (PC1) is primarily associated with electrical conductivity (EC), total dissolved solids (TDS), Ca^{2+}, Mg^{2+}, Na^+, and HCO_3^-, with localized contributions from Cl^- and SO_4^{2-}. This assemblage reflects a mineralization process predominantly controlled by water-rock interactions and the weathering of bedrock minerals, which constitute the principal mechanisms governing groundwater chemistry. In contrast, the secondary principal components are mainly characterized by turbidity, NO_3^-, K^+, SO_4^{2-}, dissolved oxygen (DO), and pH. Their relatively lower contributions indicate local and seasonal variability, likely influenced by hydrological conditions, surface-derived inputs, and, in some locations, anthropogenic activities. Notably, during the C-II campaign, the association between Cl^- and NO_3^- suggests localized anthropogenic influences, possibly related to agricultural practices or domestic wastewater inputs. Overall, these PCA results are consistent with the geochemical diagrams and hydrochemical analyses, confirming that water-rock interactions represent the dominant process controlling groundwater chemistry.

Table 5. Results of the principal component analysis

Sampling campaign	C-I			C-II			C-III	
Factors / Variables	$F_{1\text{-}1}$	$F_{2\text{-}1}$	$F_{1\text{-}2}$	$F_{2\text{-}2}$	$F_{3\text{-}2}$	$F_{1\text{-}3}$	$F_{2\text{-}3}$	$F_{3\text{-}3}$
TDS	0.92	0.08	0.97	0.03	0.06	0.97	0.03	0.10
pH	0.60	-0.61	0.65	0.35	0.51	0.20	0.54	0.50
CE	0.96	-0.37	0.98	0.26	0.0	0.95	0.03	0.16
DO	0.21	-0.66	-0.61	0.47	0.31	0.26	0.54	0.55
Turb	0.02	0.53	-0.10	0.22	0.14	0.01	0.83	-0.50
Ca^{2+}	0.91	0.31	0.89	0.08	0.20	0.77	0.29	0.07
Mg^{2+}	0.80	0.47	0.65	-0.18	-0.55	0.73	0.05	0.03
Na^{+}	0.83	0.21	0.87	0.21	0.09	0.80	0.01	0.11
K^{+}	0.04	0.56	0.56	0.11-	0.14	0.33	0.50	0.65
HCO_3^-	0.90	0.16	0.98	-0.01	-0.07	0.61	0.00	0.06
Cl^-	0.66	0.47	0.08	-0.59	-0.58	0.95	0.15	0.08
SO_4^{2-}	0.64	0.46	0.57	0.09	0.31	0.02	0.80	-0.53
NO_3^-	-0.16	0.77	0.06-	-0.51	0.52	-0.12	0.59	0.01
F^-	0.06	0.08	0.52	0.49	-0.03	0.04	0.11	0.02
Total variance	6.1	2.4	6.7	1.58	1.43	5.14	2.56	1.53
Percentage of variance	50.83	20.01	52	12.15	10.98	39.56	19.71	11.79
Cumulative percentage	50.83	70.84	52	64.15	75.12	39.56	59.27	71.06
Determinant	0.00			0.00			0.00	
Kaiser–Meyer-Olkin (KMO) measure	0.71			0.76			0.71	
Bartlett's test of sphericity (p-value)	P < 0.001			P < 0.001			P < 0.001	

3.4. Hydrochemical Classification of Groundwater

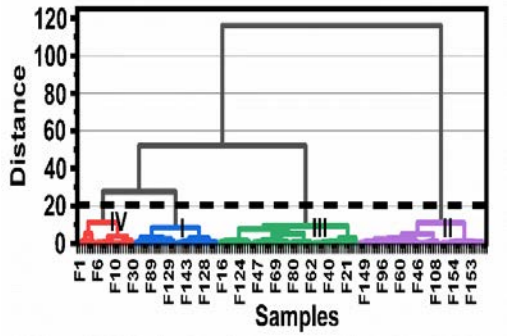
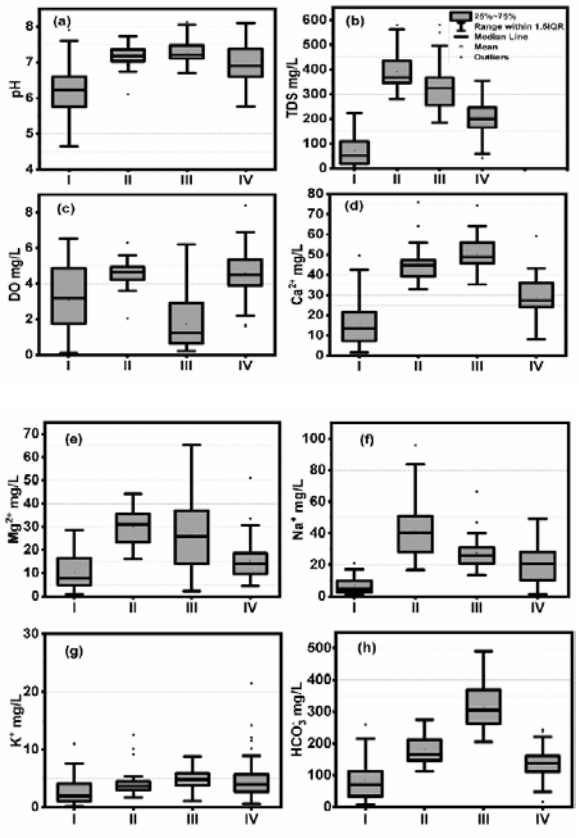


Figure 5. Dendrogram

The results of the ascending hierarchical classification (AHC) (Figure 5) are presented as a dendrogram, supplemented by box-and-whisker plots (Figure 6)illustrating the average ionic composition of each group and showing the distribution of the main hydrochemical parameters. The AHC distinguishes four groups of groundwater with contrasting hydrochemical signatures, reflecting varying degrees of mineralization and water-rock interactions [45]. The whisker plot diagrams show that Classes I and IV are dominated by Ca^{2+}, Mg^{2+}, and HCO_3^- ions, which correspond to calco-magnesian bicarbonate-type waters typical of bedrock aquifers, where mineralization is primarily controlled by the weathering of silicate minerals. Class II is characterized by a relatively higher contribution from Na^+ and K^+ ions, suggesting hydrochemical processes linked to silicate weathering and, locally, to cation exchange. Class III exhibits the highest electrical conductivities, total dissolved solids (TDS) levels, and concentrations of Cl^- and SO_4^{2-}, reflecting a more advanced stage of mineralization. Box-and-whisker plots confirm these differences between the groups. Class III has the highest median values for electrical conductivity, TDS, and most major ions, while Class I comprises the least mineralized waters. Overall, the CAH identifies four distinct hydrochemical groups, whose differences are primarily related to the degree of mineralization and the relative proportions of major ions.



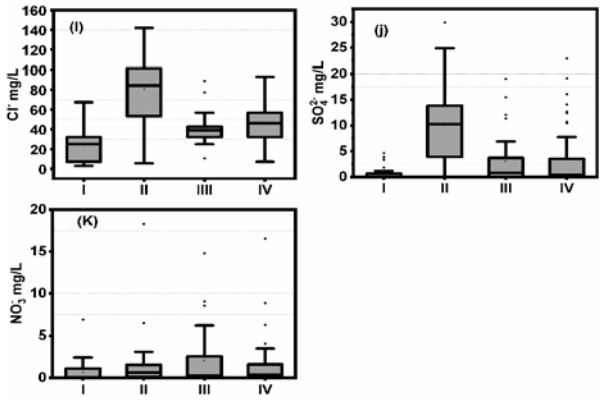
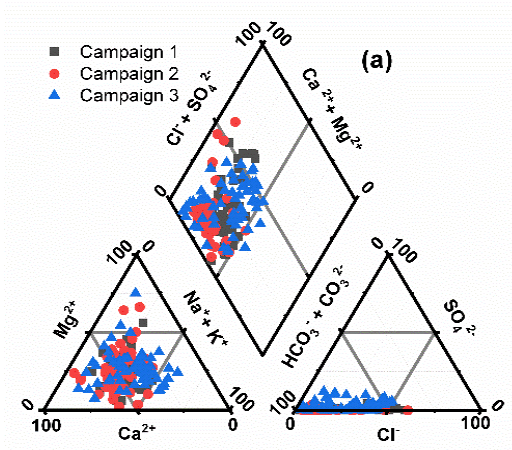


Figure 6. Whisker plots (a through k) based on hierarchical classification analysis

3.5. Hydrochemical Facies

3.5.1. Piper Diagram

The hydrochemical facies were determined based on major ion concentrations using the Piper diagram [46] (Figure 7a). The majority of samples belong to the Ca-Mg-HCO_3 facies, characteristic of bedrock aquifers, where the chemical composition is primarily controlled by water-rock interactions and the weathering of silicate minerals. This dominance is confirmed by the predominance of Ca^{2+} and Mg^{2+} ions in the cation triangle and of bicarbonates in the anion triangle. A limited number of samples shift toward a Ca-Mg-Cl facies, resulting in a relative enrichment in chlorides. A few samples from the second field campaign also show a shift toward the Cl-NO_3pole, suggesting localized surface inputs of anthropogenic origin, without exceeding the guideline values for water intended for human consumption. A comparison of the three campaigns reveals overall stability in the hydrochemical facies. The groups identified through hierarchical ascending classification (Figure 7b) are distinguished primarily by their degree of mineralization rather than by facies differences, confirming that water-rock interactions are the dominant process, with localizedanthropogenic influences.



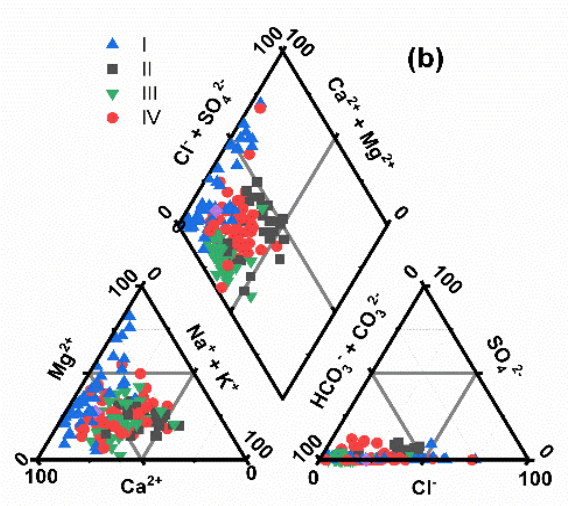


Figure 7. Piper showing the chemical composition of water

3.5.2. Durov Diagram

The Durov diagram (Figure 8) was used to clarify the hydrochemical processes that control changes in groundwater composition [47,48]. The results are consistent with those obtained from the Piper diagram and hierarchical ascending classification. The majority of samples are grouped in regions dominated by Ca^{2+}, Mg^{2+}, and HCO_3^- ions, confirming the predominance of the calcium-magnesium bicarbonate facies and the major role of water-rock interactions in the mineralization of the water. The most mineralized samples are characterized by higher electrical conductivities and total dissolved solids (TDS) concentrations, reflecting a more advanced hydrochemical evolution associated with a longer water-rock contact time. A few samples show a relative enrichment in Cl^-, SO_4^{2-}, and NO_3^-, suggesting localized surface inputs that may be associated with human activities or hydrological conditions. However, these enrichments remain limited and do not alter the dominant hydrochemical facies.

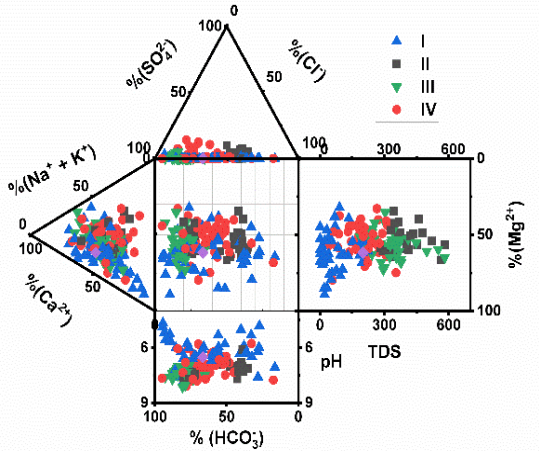


Figure 8. Durov diagrams showing the chemical composition of water

3.6. Gibbs Diagram: Mechanisms Governing Water Mineralization

The Gibbs diagram (Figure 9) was used to identify the main mechanisms controlling water chemistry, using the $Na^+/\left(Na^+ + Ca^{2+}\right)$ and $Cl^-/\left(Cl^- + HCO_3^-\right)$ ratios as a function of total dissolved solids (TDS) [13]. The majority of samples, from both groundwater and surface water, fall within the region governed by water-rock interactions, indicating that mineralization is primarily driven by the weathering of bedrock minerals. This interpretation is consistent with the predominance of the Ca-Mg-HCO_3 facies highlighted by the Piper diagram and with the results of the multivariate statistical analysis. A few samples are located near regions controlled by precipitation or by evaporation-crystallization. The former correspond to waters with the lowest mineral content, while the latter reflect local enrichment in dissolved species, likely driven by evaporation during periods of low recharge. However, their low proportion indicates that these processes play a secondary role in the hydrochemical evolution of the waters [49]. Overall, the Gibbs diagram confirms that water-rock interactions are the primary mechanism controlling the chemical composition of the basin's waters, while the effects of precipitation and evaporation remain localized. These results are consistent with those obtained from the Piper and Durov diagrams, hierarchical classification, and principal component analysis, and corroborate observations made in other bedrock aquifers in West Africa [30,50].

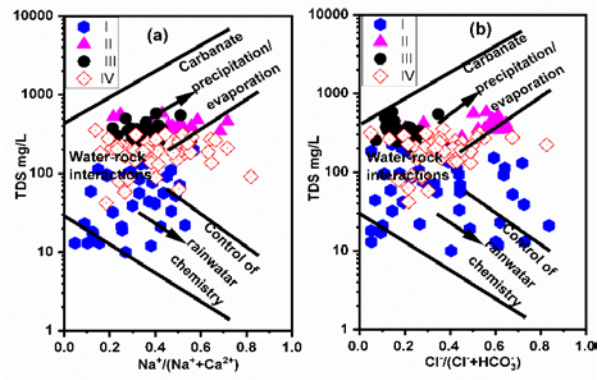


Figure 9. Gibbs diagram illustrating the general mechanisms governing the chemical composition of the waters in the Mô Basin

3.7. Geochemical Processes and the Influence of Human Activities

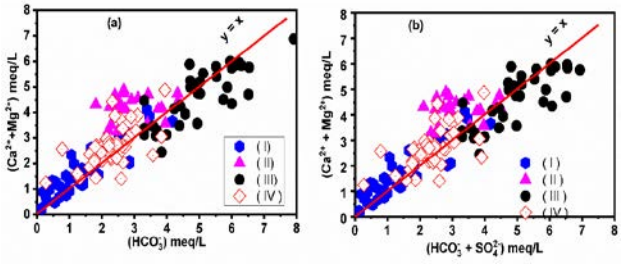
3.7.1. Geochemical Diagrams

The geochemical processes controlling groundwater chemistry were investigated using ionic relationships and geochemical diagrams [51] (Figure 10). The relationships between $(Ca^{2+} + Mg^{2+})$ and HCO_3^-, as well as between $(Ca^{2+} + Mg^{2+})$ and $(HCO_3^- + SO_4^{2-})$, indicate that most samples plot close to the theoretical 1:1 stoichiometric line (Figure 10a and Figure 10b). This distribution suggests that water-rock interactions predominantly control groundwater mineralization through the dissolution of weathering products. A limited number of samples exhibit an excess of Ca^{2+} and Mg^{2+} relative to HCO_3^- and SO_4^{2-}, indicating an additional contribution from the weathering of Ca- and Mg-bearing silicate minerals.

The weathering diagrams proposed by Gaillardet et al. (1999) (Figure 10c and Figure 10d) further support this interpretation [52,53]. Most groundwater samples fall within the silicate weathering domain, demonstrating that the hydrolysis of feldspars, amphiboles, and other aluminosilicate minerals is the dominant source of dissolved major ions. A few samples occupy an intermediate position between the silicate and carbonate end-members, suggesting a localized contribution from carbonate-rich lithological materials or secondary carbonate phases.

The Na^+/Cl^- molar ratio provides additional insight into the origin of dissolved sodium (Figure 10e). Ratios exceeding unity indicate that $Na^+$is mainly derived from the weathering of sodium-bearing silicate minerals, particularly feldspars, rather than from halite dissolution [54,55]. Conversely, Na^+/Cl^- ratios below 1 reflect a relative chloride enrichment, which may be associated with localized anthropogenic inputs, including domestic wastewater and agricultural activities.

The cation exchange process was evaluated using the relationship between $(Ca^{2+} + Mg^{2+}) - \left(HCO_3^- + SO_4^{2-}\right)$ and $\left(Na^+ - Cl^-\right)$ (Figure 10f). The inverse correlation observed between these parameters indicates active $Na^+ - Ca^{2+}/Mg^{2+}$ ion exchange between groundwater and clay minerals, suggesting that cation exchange acts as a secondary geochemical process modifying groundwater composition after primary mineral dissolution. Overall, the geochemical diagrams indicate that groundwater chemistry is primarily controlled by silicate weathering and water-rock interactions. Secondary processes, including cation exchange and localized enrichments in Cl^-, SO_4^{2-}, and NO_3^-, reflect local hydrogeochemical conditions and limited anthropogenic influences. These findings are consistent with the interpretations derived from the Gibbs, Piper, and Durov diagrams, as well as the results of the principal component analysis, highlighting the dominant role of natural geochemical processes in controlling groundwater composition within the study area.



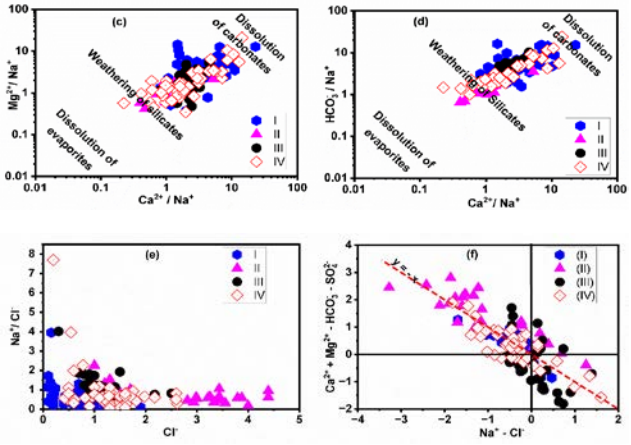


Figure 10. Binary diagrams : (a) Ca^{2+} + Mg^{2+} = f(HCO_3^-); (b) Ca^{2+} + Mg^{2+} = f (HCO_3^- + SO_4^{2-}); Gaillardet diagrams (c and d); (e) Na^+/Cl^- = f(Cl^-); (f) (Ca^{2+} + Mg^{2+}) - (HCO_3^- + SO_4^{2-}) = f(Na^+ - Cl^-).

3.7.2. Indicators of Anthropogenic Contamination

The NO_3^- / Cl^- ratio as a function of Cl^- concentration (Figure 11) was used to assess the influence of anthropogenic sources on groundwater composition [56,57]. The majority of samples exhibit an NO_3^- / Cl^- ratio of less than 1, indicating a relative predominance of chlorides over nitrates. The highest chloride concentrations are observed in Groups II and IV, suggesting the influence of diffuse sources, such as agricultural activities and domestic discharges [48,58]. Low NO_3^- / Cl^- ratios may also indicate denitrification, which is favored under reducing conditions. This interpretation is supported by the low dissolved oxygen concentrations observed in most samples, together with the relatively high iron levels, which may facilitate nitrate reduction through redox-driven reactions. Although not statistically significant, the negative correlation between total iron and nitrate concentrations is consistent with this hypothesis

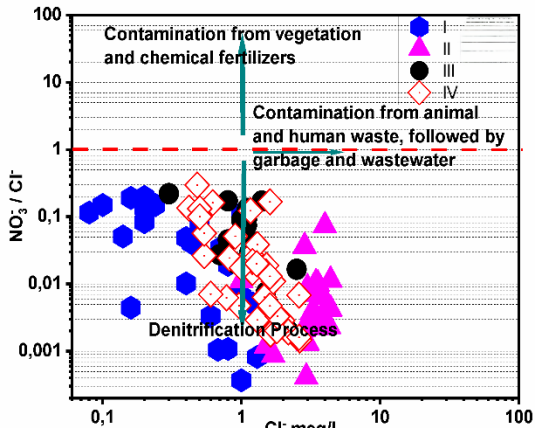


Figure 11. Anthropogenic Contamination

3.7.3. Spatial Distribution of Pollution Risk Zones

The pollution risk zoning map (Figure 12) reveals a heterogeneous spatial distribution of pollution risk across the study area. The very low-, low-,and moderate-risk classes account for 42.8%, 38.7%, and 18.5% of the total area, respectively. The very low-risk class is the most extensive and is predominantly concentrated in the central and southern parts of the study area. Low-risk zones are discontinuously distributed around these sectors. Although limited in spatial extent, moderate-risk zones occur as localized clusters, particularly within agricultural and urbanized areas in the northwestern part of the study area. This spatial pattern highlights the concentration of pollution risk in specific sectors, which should be considered priority areas for environmental monitoring and management initiatives.

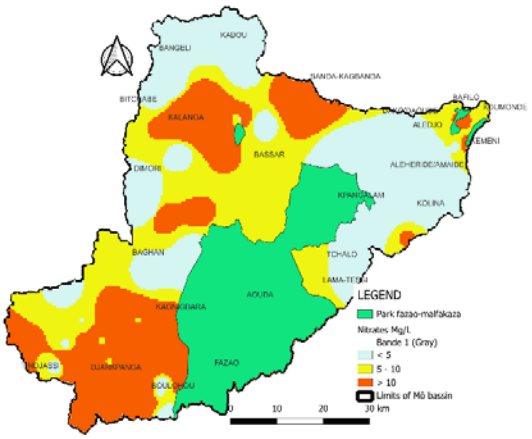


Figure 12. Pollution Risk Zoning Map

3.8. Irrigation Water Suitability

The suitability of groundwater for irrigation was assessed using the USSL (SAR-EC) and Wilcox (%Na-EC) diagrams [59] (Figure 13). The USSL diagram indicates that most samples fall within the C_1S_1 and C_2-S_1 classes, which are characterized by low salinity and low sodicity hazards. A few samples collected during the second sampling campaign are distributed within the C_2-C_3 classes, reflecting a slight increase in water mineralization. However, SAR values remain within the S_1-S_2 classes, indicating a limited risk of clay dispersion and soil structural degradation.

The Wilcox diagram corroborates these findings. Most samples are classified as Excellent to Good, whereas only a limited number fall into the Permissible category, mainly during the second sampling campaign. The moderate %Na values indicate a low risk of soil sodification.

The differences observed between the two sampling campaigns highlight the influence of the hydrological regime on groundwater quality. During low-flow periods, dissolved salts tend to become more concentrated, whereas recharge periods favor the partial dilution of dissolved ions, leading to slight variations in groundwater mineralization. However, these seasonal fluctuations do not significantly alter the overall classification of groundwater suitability for irrigation. [60,61,62].

Overall, both the USSL and Wilcox diagrams indicate that groundwater in the Mô Basin is generally suitable for irrigation. The low salinity and sodicity levels suggest a limited risk of soil salinization and sodification. However, seasonal monitoring is recommended to detect potential changes in water quality and to prevent future degradation in the most vulnerable areas.

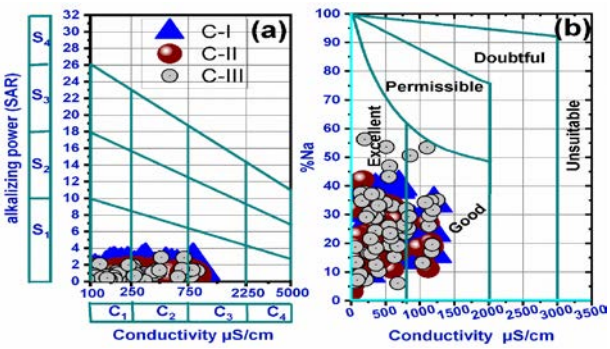


Figure 13. Irrigation Suitability of Groundwater in the Mô Basin

4. Conclusion

This study investigated the hydrochemical characteristics of groundwater and surface water in the Mô Basin using physicochemical analyses, multivariate statistical techniques, and geochemical approaches. The results indicate that water chemistry is predominantly characterized by the Ca-Mg-HCO_3 hydrochemical facies, typical of aquifers developed within crystalline and metamorphic formations. The Piper, Durov, and Gibbs diagrams, ionic ratios, saturation indices, and multivariate statistical analyses consistently demonstrate that silicate weathering is the dominant process controlling water mineralization, whereas cation exchange acts as a secondary geochemical mechanism. Evaporite minerals exert only a minor influence on water chemistry, while carbonate minerals are generally close to thermodynamic equilibrium. Seasonal variations primarily affect the degree of mineralization without significantly altering the dominant hydrochemical facies. Higher concentrations of dissolved ions observed during the dry season reflect concentration effects associated with reduced groundwater recharge and enhanced evaporation, whereas the rainy season promotes the dilution of dissolved constituents. Localized enrichments in chloride, sulfate, and nitrate concentrations suggest sporadic anthropogenic inputs, most likely associated with agricultural practices and domestic wastewater discharges; however, these influences remain secondary to the prevailing geogenic processes.

The assessment of irrigation water suitability indicates that the water resources are generally suitable for agricultural use. Hydrochemical indices, combined with the USSL and Wilcox diagrams, indicate that most samples present low salinity and sodicity risks, suggesting their suitability for a wide range of irrigation practices. Nevertheless, the seasonal increase in the hydrochemical indices during the dry season highlights the need for appropriate water management strategies to minimize the risks of soil salinization and sodification.

Overall, this study provides an integrated understanding of the hydrochemical processes governing water quality in the Mô Basin and offers valuable scientific evidence to support the sustainable management of its water resources. Future research incorporating trace elements, environmental isotopes, and long-term hydrochemical monitoring would improve the identification of mineralization sources and provide a better assessment of the impacts of land-use change and climate variability on water quality.

References

[1] M. S. Forde, A. Cashman, et K. Mitchell, «Sustainability of water resources in Caribbean small island developing states: an overview», Discov Sustain, vol. 5, no. 1, p. 265, Sept. 2024.

[2] UNESCO, 'United Nations World Water Development Report 2024, Water for.' Accessed: July 5, 2026. [Online]. Available at: https://www.unesco.org/en/articles/united-nations-world-water-development-report-2024-water-prosperity-and-peace.

[3] A.-S. Msl, T. I, C. H, B. Gd, et B. Lm, «Hydrochemical Control of Groundwater Quality in an Urban Area of Lome Aquifer, Togo», International Journal of Chemical Sciences, vol. 15, n° 4, p. 1-8, Nov. 2017.

[4] UNESCO, "Groundwater: Making the Invisible Visible | United Nations World Water Development Report 2022." Accessed: July 5, 2026. [Online]. Available at: https:// www.unesco.org/ reports/wwdr/2022.

[5] C. A. J. Appelo et D. Postma, Geochemistry, Groundwater and Pollution, 2e éd. London: CRC Press, 2004.

[6] Y. Liu, J. Zhang, Z. Bao, Y. Yang, et G. Wang, «Hydrological Change Detection and Process Simulation for a Semi-Arid Catchment in Northern China», Water, vol. 14, n°. 8, Art. n°. 8, Janv. 2022.

[7] WHO, «Guidelines for Drinking-water Quality, 4th edition incorporating the second addendum. World Health Organization, Geneva.» 2022.

[8] D. Odeloui et al., «Insight into Groundwater Resources along the Coast of Benin (West Africa) through Geochemistry and Isotope Hydrology; Recommendations for Improved Management», Water, vol. 14, n°. 14, p. 2154, Janv. 2022.

[9] A. A. Ako et al., «Evaluation of groundwater quality and its suitability for drinking, domestic, and agricultural uses in the Banana Plain (Mbanga, Njombe, Penja) of the Cameroon Volcanic Line» Environ Geochem Health, vol. 33, no. 6, pp. 559-575, Dec. 2011.

[10] A.-S. Seyf-Laye, «Nitrate in drinking water: A major polluting component of groundwater in gulf region aquifers, south of Togo», International Journal of Physical Sciences, vol. 7, p. 144-152, Janv. 2012.

[11] K. V. Akpataku et al., «Hydrochemical and isotopic characterization of groundwater in the southeastern part of the Plateaux Region, Togo», Hydrological Sciences Journal, vol. 64, n°. 8, p. 983-1000, Juin 2019.

[12] A. K. Sodomon et al., «Assessment of hydrogeochemical evolution of groundwater from the basement aquifer in the upper part of transboundary Mono River Basin, Togo», Journal of Hydrology: Regional Studies, vol. 58, p. 102200, avr. 2025.

[13] R. J. Gibbs, «Mechanisms Controlling World Water Chemistry», Science, vol. 170, n°. 3962, p. 1088-1090, déc. 1970.

[14] M. Velis, K. I. Conti, et F. Biermann, «Groundwater and human development: synergies and trade-offs within the context of the sustainable development goals», Sustain Sci, vol. 12, n°. 6, p. 1007-1017, 2017.

[15] Y. Akakpo, A. Bleza, G. Boguido, K. Zouari, R. Trabelsi, and M. D.-T. Gnazou, 'Hydrogeochemical Evaluation of the Volta Basin Aquifers: Case of the Upper Oti Sub-Basin in Togo,' Afrique SCIENCE, vol. 26, no. 2, pp. 91-104, 2025.

[16] F. Wang et al., «Solute Geochemistry and Water Quality Assessment of Groundwater in an Arid Endorheic Watershed on Tibetan Plateau», Sustainability, vol. 14, n° 23, p. 15593, déc. 2022.

[17] P. G. Whitehead et al., «Water quality modelling of the Mekong River basin: Climate change and socioeconomics drive flow and nutrient flux changes to the Mekong Delta», Science of the Total Environment, vol. 673, p. 218-229, juill. 2019.

[18] Y. Oyda, S. D. Hatiye, and M. Jothimani, "Evaluation of Groundwater Quality for Drinking and Irrigation Purposes Using Entropy-Weighted WQI, Pollution Index, and Multivariate Statistical Analysis in the Maze Zenti Catchment, Southern Ethiopia," Geosciences, vol. 16, no. 1, p. 50, Jan. 2026.

[19] E. Manu, M. De Lucia, et M. Kühn, «Hydrochemical characterization of surface water and groundwater in the crystalline basement aquifer system in the Pra Basin (Ghana)»,

Water, vol. 15, n°. 7, p. 1325, 2023.

[20] R. R. Pant et al., «Hydrochemical characteristics and water quality assessment of surface water in the Badigad River Basin, Lesser Himalayas, Nepal», Environ Sci Pollut Res, vol. 32, n°. 33, p. 19836-19859, juill. 2025.

[21] L. Duan et al., «Identifying the spatio-seasonal pattern of hydrochemical evolution and surface water-groundwater interaction in a large urban river basin, Northwest China», Science of the Total Environment, vol. 944, p. 173989, Sept. 2024.

[22] C. Millogo, A. Sako, B. Sagnon, et S. Nakolendousse, «Hydrochemical and spatial assessment of groundwater quality from fractured basement aquifers in the south-central part of Burkina Faso, West Africa», West Africa, 2024, Accessed on: September 27, 2026. [Online]. Available at: https:// papers.ssrn.com/sol3/papers.cfm?abstract_id=4950052.

[23] Simpara, N. (1978) Geological and structural study of the external units of the Pan-African chain (600 Ma) of the Dahomeyides in the Bassar region (Togo). 3rd cycle thesis, University of Aix-Marseille-III, Marseille, 164 p. - References - Scientific research publication." Accessed on: July 6, 2026. [Online]. Available at: https://www.scirp.org/reference/referencespapers?referenceid=33200977.

[24] Lamouroux, M. (1969) Explanatory note on the soil map of Togo. ORSTOM, Paris, 86 p. - References - Scientific research publication.' Accessed on: July 6, 2026. [Online]. Available at: https://www.scirp.org/reference/referencespapers?referenceid=2669087.

[25] P. Affaton, M. A. Rahaman, R. Trompette, et J. Sougy, «The Dahomeyide Orogen: Tectonothermal Evolution and Relationships with the Volta Basin», in The West African Orogens and Circum-Atlantic Correlatives, R. D. Dallmeyer et J. P. Lécorché, Éd., Berlin, Heidelberg: Springer Berlin Heidelberg, 1991, p. 107-122.

[26] P. Lachassagne, B. Dewandel, et R. Wyns, «Review: Hydrogeology of weathered crystalline/hard-rock aquifers—guidelines for the operational survey and management of their groundwater resources», Hydrogeol J, vol. 29, n° 8, p. 2561-2594, déc. 2021.

[27] K. Z. Houédakor et D. Yamoula, «Analysis of Hydro-Climatical Variability in the Mo Basin in Togo», JWARP, vol. 13, n°. 12, p. 1043-1060, 2021.

[28] K. O. Doro, P. I. Olabode, M. A. Adeniran, et M. A. Oladunjoye, «Understanding Complex Hydraulic Heterogeneities in Crystalline Basement Aquifers Used as Drinking Water Sources», Geosciences, vol. 15, n°. 7, p. 239, juill. 2025.

[29] E. D. Sunkari, J. Seidu, et A. Ewusi, «Hydrogeochemical evolution and assessment of groundwater quality in the Togo and Dahomeyan aquifers, Greater Accra Region, Ghana», Environmental Research, vol. 208, p. 112679, mai 2022.

[30] A. K. Sodomon et al., «Assessment of hydrogeochemical evolution of groundwater from the basement aquifer in the upper part of transboundary Mono River Basin, Togo», Journal of Hydrology: Regional Studies, vol. 58, p. 102200, avr. 2025.

[31] W. Al-Zubari, A. Al-Shaabani, et N. Abdulhameid, «Spatial Optimization of the Groundwater Quality Monitoring Network in the Kingdom of Bahrain», Water, vol. 15, n° 12, p. 2169, juin 2023.

[32] L. Tampo, I. Kaboré, E. H. Alhassan, A. Ouéda, L. M. Bawa, et G. Djaneye-Boundjou, «Benthic Macroinvertebrates as Ecological Indicators: Their Sensitivity to the Water Quality and Human Disturbances in a Tropical River», Front. Water, vol. 3, Sept. 2021.

[33] AFNOR, «AFNOR, 2024. NF EN ISO 5667-3. Water quality-Sampling-Part 3: Preservation and handling of water samples. French Standardization Association, La Plaine Saint-Denis, France.» 2024

[34] D. Granato, J. S. Santos, G. B. Escher, B. L. Ferreira, et R. M. Maggio, «Use of principal component analysis (PCA) and hierarchical cluster analysis (HCA) for multivariate association between bioactive compounds and functional properties in foods: A critical perspective», Trends in Food Science & Technology, vol. 72, p. 83-90, févr. 2018.

[35] D. H. F. Muniz et E. C. Oliveira-Filho, «Multivariate Statistical Analysis for Water Quality Assessment: A Review of Research Published between 2001 and 2020», Hydrology, vol. 10, n°. 10, p. 196, Oct. 2023.

[36] WHO, « Guidelines for drinking-water quality: fourth edition incorporating the first and second addenda ». Accessed on: July 5, 2026. [Online]. Available at: https:// www.who.int/ publications/ i/item/9789240045064.

[37] K. V. Akpataku et al., «Hydrogeochemical Characteristics of Groundwater in the Prefecture of Bassar, Togo», Am. J. Chem. Eng., vol. 13, n° 1, p. 1-13, janv. 2025.

[38] X. Wang et al., «Hydrochemical Characteristics and Genesis of Groundwater in Taoshan Granite Body, Yushan Uplift Area, South Jiangxi, China», Water, vol. 17, n°. 7, p. 974, Apr. 2025.

[39] Y. Zhang et al., «Lithological Controls on Chemical Weathering and CO_2 Consumption at Small Watershed Scale : Insights from Hydrochemistry and Stable Carbon Isotope», Water, vol. 17, n° 13, p. 2008, juill. 2025.

[40] K. K. Agrawal, C. Panda, et M. K. Bhuyan, «Impact of Urbanization on Water Quality», in Current Advances in Mechanical Engineering, S. K. Acharya et D. P. Mishra, Éd., Singapore: Springer Singapore, 2021, p. 665-673.

[41] M. Cabrera et al., «Effects of intensive agriculture and urbanization on water quality and pesticide risks in freshwater ecosystems of the Ecuadorian Amazon», Chemosphere, vol. 337, p. 139286, Oct. 2023.

[42] W. Qiao et al., «Groundwater arsenic and antimony mobility from an antimony mining area: Controls of sulfide oxidation, carbonate and silicate weathering, and secondary mineral precipitation», Water Research, vol. 273, p. 123086, avr. 2025.

[43] M. B. Moussa, "Surface Water Quality in the Niamey Area: Physicochemical Characterization and Spatiotemporal Dynamics of Suspended Solids (SS) and Fecal Bacteria (E. coli) Concentrations," Ph.D. thesis, Paul Sabatier University-Toulouse III; Abdou Moumouni University, 2023.

[44] X. Wang et al., «Source Analysis of Groundwater Chemical Components in the Middle Reaches of the Dawen River Based on Unsupervised Machine Learning and PMF Source Analysis», Water, vol. 17, n°. 20, p. 2924, Oct. 2025.

[45] U. Basharat et al., «Integrated assessment of groundwater hydrogeochemistry and quality using multivariate statistical analysis, self-organizing maps, and water quality indices in District Bagh, AJK, Pakistan», Ecotoxicology and Environmental Safety, vol. 301, p. 118515, août 2025.

[46] S. Ali et al., «Groundwater quality assessment using water quality index and principal component analysis in the Achnera block, Agra district, Uttar Pradesh, Northern India», Sci Rep, vol. 14, n°. 1, p. 5381, mars 2024.

[47] A. M. Auwal et al., «Integrated hydrogeochemical and multivariate statistical assessment of groundwater in Gashua, northeastern Nigeria: implications for arid zone aquifer management», Model. Earth Syst. Environ., vol. 12, n° 2, p. 95, févr. 2026.

[48] G. Sharma, R. Lata, N. Thakur, V. Bajala, J. C. Kuniyal, et K. Kumar, «Application of multivariate statistical analysis and water quality index for quality characterization of Parbati River, Northwestern Himalaya, India», Discov Water, vol. 1, n°. 1, p. 5, Sept. 2021.

[49] L. Tampo et al., «Treated wastewater suitability for reuse in comparison to groundwater and surface water in a peri-urban area: Implications for water quality management», Science of the Total Environment, vol. 815, p. 152780, avr. 2022.

[50] M. Ani, J. Junuat, B. Marin, and K. Gnandi, «Hydrochemical and Isotopic Characterization of Groundwater in the Kara River Watershed (Northern Togo)» ResearchGate. Accessed April 7, 2026. [Online]. Available at: https://www.researchgate.net/publication/366052472

[51] A. Shuaibu, R. M. Kalin, V. Phoenix, et I. M. Lawal, «Geochemical evolution and mechanisms controlling groundwater chemistry in the transboundary Komadugu–Yobe Basin, Lake Chad region: An integrated approach of chemometric analysis and geochemical modeling», Journal of Hydrology: Regional Studies, vol. 57, p. 102098, Févr. 2025.

[52] J. Gaillardet, B. Dupré, P. Louvat, et C. J. Allègre, «Global silicate weathering and CO_2 consumption rates deduced from the chemistry of large rivers», Chemical Geology, vol. 159, n° 1-4, p. 3-30, Juill. 1999.

[53] K. V. Akpataku et al., «Hydrogeochemical Characteristics of Groundwater in the Prefecture of Bassar, Togo», Am. J. Chem. Eng., vol. 13, n° 1, p. 1-13, janv. 2025.

[54] M. Magaritz, A. Nadler, H. Koyumdjisky, et J. Dan, «The use of Na/Cl ratios to trace solute sources in a semiarid zone», Water Resources Research, vol. 17, n° 3, p. 602-608, juin 1981.

[55] A. Bourjila, «Hydrochemical Modeling of Marine Intrusion into

the Ghiss-Nekor Coastal Aquifer and Characterization of Potential Groundwater Zones in the Ghiss and Nekor Watersheds (Morocco) Using Geospatial Methods,» Ph.D. thesis, Abdelmalek Essaâdi University (Tetouan, Morocco), 2023. Accessed: September 27, 2026. [Online]. Available at: https://hal.science/tel-04553629.

[56] Q. Zhang, H. Qian, P. Xu, K. Hou, et F. Yang, Groundwater quality assessment using a new integrated-weight water quality index (IWQI) and driver analysis in the Jiaokou Irrigation District, China», Ecotoxicology and Environmental Safety, vol. 212, p. 111992, Apr. 2021.

[57] B. Zhou, H. Wang, et Q. Zhang, « Assessment of the Evolution of Groundwater Chemistry and Its Controlling Factors in the Huangshui River Basin of Northwestern China, Using Hydrochemistry and Multivariate Statistical Techniques », International Journal of Environmental Research and Public Health, vol. 18, n°. 14, p. 7551, Jul. 2021.

[58] K. V. Akpataku et al., «Hydrochemical and isotopic characterization of groundwater in the southeastern part of the Plateaux Region, Togo», Hydrological Sciences Journal, vol. 64, n°. 8, p. 983-1000, Juin 2019.

[59] S. Pawar et R. Bhagat, «Assessment of Groundwater Hydrochemistry and Irrigation Suitability Using Piper, Wilcox, and USSL Diagrams in the Sina River Basin», International Journal of Scientific Research in Science, Engineering and Technology, vol. 13, n°. 3, p. 164-174, May 2026.

[60] S. A. Schroeter et al., «Hydroclimatic extremes threaten groundwater quality and stability», Nat Commun, vol. 16, n°. 1, p. 720, Janv. 2025.

[61] M. Ullengula et al., «Seasonal controls on groundwater irrigation quality in a semi-arid granitic watershed of Telangana, India: an integrated IWQI-GIS-multivariate approach», Sci Rep, vol. 16, no. 1, p. 16631, avr. 2026.

[62] D. Kim, J. Lu, M. E. Roberts, D. T. Roberts, D. N. Orr, et D. P. Hamilton, «Groundwater levels, climate and anthropogenic factors affect the hydrology and water quality of an intermittent and a regulated subtropical stream», Hydrological Processes, vol. 38, n°. 1, p. e15074, 2024.



© The Author(s) 2026. This article is an open access article distributed under the terms and conditions of the Creative Commons Attribution (CC BY) license (http://creativecommons.org/licenses/by/4.0/).